Soft Matter

Accepted Manuscript

ROYAL SOCIETY OF CHEMISTRY

www.rsc.org/softmatter

Cite this: DOI: 10.1039/c0xx00000x

www.rsc.org/xxxxxx

ARTICLE TYPE

Biocompatible Cationic Lipids for the Formulation of Liposomal DNA vectors

Costanza Montis,[a] Silvia Sostegni,[a,b] Silvia Milani,[a,c] Piero Baglioni[a] and Debora Berti*[a]

Received (in XXX, XXX) Xth XXXXXXXXX 20XX, Accepted Xth XXXXXXXXX 20XX

DOI: 10.1039/b000000x

Ethylphosphocholine lipids are highly biocompatible cationic amphiphiles that can be used for the formulation of liposomal DNA vectors, with negligible toxic side effects on cells and organisms. Here we report a characterization of EDPPC (1,2-Dipalmitoyl-sn-glycero-O-ethyl-3-phosphocholine, chloride) liposomes, containing two different zwitterionic helper lipids, POPC (1-Palmitoyl-2-oleoyl-sn-glycero-3-phosphocholine) and DOPE (1,2-dioleoyl-sn-glycero-3-phosphoethanolamine). Depending on the nature of the helper lipid, a phase separation in the bilayer is found at room temperature, where domains enriched in the cationic component coexist in a relatively large temperature range with regions where the zwitterionic lipids is predominant. We studied DNA complexation, the internal structure of lipoplexes and their docking and fusogenic ability with model target bilayers. The structural and functional modifications caused by DNA binding were followed with Dynamic Light Scattering (DLS), Zeta Potential, Small and Wide Angle X-Ray Scattering (SAXS-WAXS), while the interaction with membranes was assessed by using Giant Unilamellar Vesicles (GUVs) as model target bilayers. The results presented establish a connection between the physicochemical properties of lipid bilayers, and in particular of lipid demixing, on the phase state of the complexes and their ability to interact with model membranes.

Introduction

Nucleic acids interfere with gene expression in cells. This ability has determined a growing interest in the design and development of new drugs or prodrugs based on DNA or RNA (i.e. plasmids containing transgenes,[1,2] oligonucleotides,[3] ribozymes, aptamers[4] and small interfering RNA (si-RNA)).[5] Gene therapy has the potential to become the most powerful approach for the treatment of a wide range of diseases, such as cancer, AIDS, microbial infections, neurodegenerative diseases and cardiovascular disorders. Genetic drugs selectively recognize their molecular targets, providing a more specific strategy for medical treatment than traditional drugs. However, advancement in this field is currently limited by several issues, primarily by the need of suitable vectors for the drug that protect the genetic material from degradation and enhance cell internalization and drug release (transfection). Viral carriers have these properties, but they also elicit a strong immune response[6,7] and pose severe safety concerns, which have prompted the requirement of alternative synthetic delivery systems.

In this area, the leading role is held by cationic liposomes, composed of synthetic cationic lipids. DNA is complexed due to electrostatic compensation, and its conformation changes from the native to a condensed form, where it is protected from degradation operated by nucleases.[8,9] The presence of a lipid liquid crystalline phase in the complex improves the membrane affinity and tune the fusogenic properties with target cells.

Several cationic liposomal formulations have been proposed, characterized and tested in a wide range of tissues; the vast majority of these reports concerns cationic liposomes where DOTAP (1,2-dioleoyl-3-trimethylammonium-propane) is the active ingredient. Although relatively efficient *in vitro*, those liposomes show high cytotoxicity, which limits their application *in vivo*.[10]

Ethylphosphocholine are very similar to natural phosphocholines, but with an additional ethyl ester on the phosphate group (see Scheme 1), whose presence imparts a net positive charge to the headgroup. Their polar head can be hydrolyzed by phospholipases and metabolized in cell cultures.[11] As natural phospholipids, they are therefore sensitive to the enzymatic machinery and do not accumulate in cells and tissues. Ethylphosphocholines are very promising amphiphiles for the efficient and safe delivery of nucleic acids, because of the very low toxic side effects on organisms.[12–17] A number of reports have addressed the structure–activity relationship for lipofection in ethylphosphocholine formulations. In particular, the unsaturation and length of the acyl chains[18] and the addition of zwitterionic or other kinds of cationic lipids,[19,20] proved to be relevant parameters for the transfection efficiency.

Despite these progresses, the investigation on these systems is surprisingly limited with respect to DOTAP, which is still the cationic lipid of choice for DNA vectors[21–23] notwithstanding its established toxicity.[24–26]

In particular, very few studies[27,19] addressed the effect of the addition of helper lipids on ethylphosphocholine-based

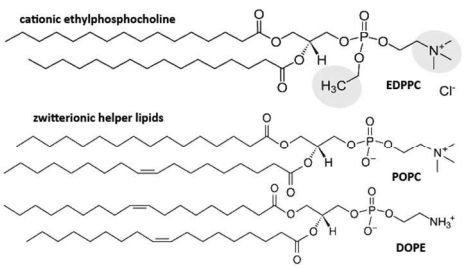

Scheme 1 Molecular structure of the cationic ethylphosphocholine EDPPC (1,2-dipalmitoyl-sn-glycero-3-ethylphosphocholine (chloride salt)) and of the zwitterionic helper lipids POPC (1-Palmitoyl-2-oleoyl-sn-glycero-3-phosphocholine) and DOPE (1,2-dioleoyl-sn-glycero-3-phosphoethanolamine).

liposomes. Zwitterionic helper lipids are added to cationic liposomal formulations to modulate surface charge, colloidal stability and ability to bind nucleic acids. Moreover they determine the nature of the internal liquid crystalline phase of the complexes with DNA (lipoplexes), and consequently the fusogenic ability of the vectors with the cell membrane for internalization.

To address this point, here we investigate cationic liposomes from EDPPC (1,2-Dipalmitoyl-sn-glycero-O-ethyl-3-phosphocholine chloride), mixed with two different helper lipids, POPC (1-Palmitoyl-2-oleoyl-sn-glycero-3-phosphocholine) and DOPE (1,2-dioleoyl-*sn*-glycero-3-phosphoethanolamine), see Scheme 1. POPC has the same cationic group as EDPPC, i.e. a choline, while DOPE has an ethanolamine moiety on the headgroup; the first lipid has one unsaturated chain, while in DOPE both chains are unsaturated. These factors affect the spontaneous curvature of the lipids, which is zero for POPC and negative for DOPE.

The physicochemical and phase properties of the lipid mixtures were investigated with Differential Scanning Calorimetry (DSC) and Small Angle and Wide Angle X-Ray Scattering (SAXS-WAXS). DNA complexation, and the structural properties of lipoplexes were studied through Dynamic Light Scattering (DLS), Circular Dichroism (CD), SAXS and Zeta Potential measurements. Finally, Confocal Laser Scanning Microscopy (CLSM) shed light on the interaction between the lipoplexes and Giant Unilamellar Vesicles (GUVs), intended as a model for cell membranes. The ensemble of experimental data allows to single out the key factors affecting DNA encapsulation, and to correlate the physicochemical properties of the lipid vectors with their ability to interact with lipid membranes.

Materials and Methods

EDPPC (1,2-dipalmitoyl-sn-glycero-3-ethylphosphocholine (chloride salt)), POPC (1-Palmitoyl-2-oleoyl-sn-glycero-3-phosphocholine), DOPE (1,2-dioleoyl-sn-glycero-3-phosphoethanolamine), sketched in Scheme 1, were purchased from Avanti Polar Lipids (Alabaster, AL), such as the fluorescent probes NBD-PE (1,2-dipalmitoyl-sn-glycero-3-phosphoethanolamine-N-(7-nitro-2-1,3-benzoxadiazol-4-yl) (ammonium salt) and Liss Rhod PE (1,2-dioleoyl-sn-glycero-3-phosphoethanolamine-N-(lissaminerhodamine B sulfonyl) (ammonium salt)) and POPG (1-Palmitoyl-2-oleoyl-sn-phosphatidyl-glycerol) employed for confocal microscopy experiments.

Hepes (4-(2-Hydroxyethyl)piperazine-1-ethanesulonic-acid) was purchased from Fluka (Buchs, Switzerland). CH_3OH, $CHCl_3$ and DNA (deoxyribonucleic acid sodium salt from calf thymus, type I, highly polymerized) were provided by Sigma-Aldrich (St. Louis, MO).

Liposome Preparation.

The lipid mixtures were prepared by dissolving the required amounts of EDPPC and DOPE or POPC in chloroform/methanol 6:1 (v/v). The lipid films were obtained by evaporating the solvent under a stream of nitrogen and dried under vacuum overnight. Warm (60°C) Hepes buffer 10 mM pH 7.4 was then added, and the lipid films swollen with vigorous vortex mixing. These multilamellar vesicles (MLV) were used without further manipulation for SAXS and DSC experiments. For DLS, Zeta Potential, CLSM and CD measurements, the MLV were subjected to 10 freeze-thaw cycles and extruded 10 times through two stacked polycarbonate membranes with 100 nm pore size at 60°C, to obtain unilamellar vesicles (ULV) with narrow and reproducible size distribution. The filtration was performed with The Extruder (Lipex Biomembranes, Vancouver (Canada)) through Nuclepore membranes. For Confocal Microscopy, the liposomes were labelled with NBD-PE 0.5% mol/mol with respect to total lipid concentration. NBD-PE in chloroform was evaporated in a glass vial under a stream of N_2 and then kept under vacuum for two hours to remove the solvent traces. A dispersion of POPC:EDPPC 1:1 or DOPE:EDPPC 1:1 ULV in Hepes 10 mM (pH 7.4) was then added to the dry film and the solution was stirred overnight.

GUVs preparation: Giant Unilamellar Vesicles were prepared through electroformation.[28,29] POPC 2.5 mg/ml and POPC:POPG 1:1 mol/mol (2.5 mg/ml total lipid concentration) stock solutions in $CHCl_3$ were prepared and 0.1% (mol/mol) of the fluorescent dye Liss Rhod PE was added. 20 µl of the stock solution were deposited onto the conductive side of two glass sheets covered with ITO (10 µl on each sheet). Chloroform was dried under vacuum for two hours and a dry lipid film was obtained. The electroformation chamber was prepared separating the conductive sides of the glass sheets with an O-ring; the chamber was then filled with of 15 mM Sucrose solution, and the electrical contact was obtained by attaching a copper tape connected to a pulse generator. A sine wave of 10 Hz and 2 Vpp was applied for two hours.

Complexation with DNA: A stock solution of DNA in Hepes buffer 10 mM (pH 7.4) and stock solutions of ULV from POPC:EDPPC or DOPE:EDPPC in Hepes buffer 10 mM (pH 7.4) were diluted with the same buffer to obtain the concentrations used for DLS, Zeta potential and CD experiments: DNA $5x10^{-5}$ M and liposomes POPC:EDPPC and DOPE:EDPPC 1:1 to obtain the desired P/N positive to negative charges ratios (e.g. $1x10^{-4}$ M for P/N=1). In addition, lipoplexes were also prepared from more concentrated solutions (DNA=$1.75x10^{-4}$ M). The lipoplexes were prepared according to the following protocol: diluted solutions of liposomes and DNA in Hepes 10mM (pH 7.4) were separately incubated at room temperature for 5 minutes; the liposomal dispersion was then added to the

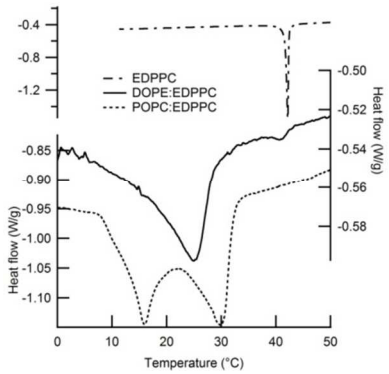

Fig. 1 DSC thermograms obtained for pure EDPPC and for POPC:EDPPC 1:1 mol:mol (dashed line) and DOPE:EDPPC 1:1 mol:mol (continuous line) lipid mixtures 400 mg/ml in Hepes 10mM pH 7.4 with a 0.5°C/min heating ramp.

DNA solution and the sample was incubated for 20 minutes at room temperature before measurements. For SAXS measurements, higher concentrations both of ULV (20 mg/ml) and of DNA, are required. In this case, after the incubation time, a precipitate was obtained. This precipitate was transferred in a demountable sample holder with two Kapton windows and measured.

Differential Scanning Calorimetry: DSC measurements were performed on a DSC Q1000 from TA Instruments. DOPE:EDPPC 1:1 and POPC:EDPPC 1:1 MLV (400 mg/ml) in 10mM Hepes were prepared as previously described. The measurements were performed with the following temperature program: equilibration at -20°C and then heating ramp from -20°C to 60°C at 0.5°C/min.

Dynamic Light Scattering: DLS measurements were performed on a Brookhaven Instruments apparatus (BI 9000AT correlator and BI 200 SM goniometer). The signal was detected by an EMI 9863B/350 photomultiplier. The light source was the second harmonic of a diode Nd:YAG laser, λ=532 nm Coherent Innova, linearly polarized in the vertical direction. The time autocorrelation functions of the intensity of the scattered light were measured at 90° and analyzed according to the Siegert relationship (eq. 1), which connects the first order or field normalized autocorrelation function $g_1(q,\tau)$ to the measured normalized time autocorrelation function $g_2(q,\tau)$:

$$g_2(q,\tau) = 1 + \beta|g_1(q,\tau)|^2 \quad (1)$$

where β is a spatial coherence factor dependent on the geometry of the detection system.

The functions $(\beta|g_1(q,\tau)|^2)^{1/2}$ were also normalized to vary between 0 and 1 for displaying purposes. The field autocorrelation functions light were analyzed through a cumulant analysis stopped to the second order.[30]

Zeta Potential: Zeta potential measurements were carried out using a Zeta Potential Analyzer (Zeta Plus, Brookhaven Instruments Corporation, Holtsville, NY). Zeta potential values were obtained from the electrophoretic mobility u, according to Helmholtz-Smoluchowski equation:

$$\zeta = {}^{\eta}/_{\varepsilon} \times u \quad (2)$$

with η being the viscosity of the medium, ε dielectric permittivity of the of dispersing medium. This equation is valid in the limit: $\kappa \times R \gg 1$, with κ^{-1} Debye length and R hydrodynamic radius of the particles. Zeta Potential values reported are averaged values obtained from 15 measurements carried out for each sample.

Circular Dichroism: Circular Dichroism measurements were carried out with a Jasco J-715 spectropolarimeter. Samples prepared in Hepes 10 mM at pH 7.4 were placed in a cuvette of 1 cm path length. Spectra were taken as the average of ten accumulations from 220 to 350 nm. The scan rate was 50 nm/min.

SAXS-WAXS: SAXS and WAXS measurements were carried out on a S3-MICRO SAXS/WAXS instrument (HECUS GmbH, Graz, Austria) which consists of a GeniX microfocus X-ray sealed Cu K_α source (Xenocs, Grenoble, France) power 50 W which provides a detector focused X-ray beam with λ = 0.1542 nm Cu K_α line. The instrument is equipped with two one-dimensional (1D) position sensitive detectors (HECUS 1D-PSD-50 M system), each detector is 50 mm long (spatial resolution 54 μm/channel, 1024 channels) and covers the SAXS Q-range (0.003 < Q < 0.6 Å−1) and the WAXS Q-range (1.2 < Q < 1.9 Å−1). The temperature was controlled by means of a Peltier TCCS-3 Hecus. SAXS-WAXS spectra were recorded on POPC:EDPPC 1:1 and DOPE:EDPPC 1:1 400 mg/ml MLV at different temperatures with the following temperature program: equilibrate to 25°C for three hours, cool stepwise at 5°C equilibrating each 5°C-step for 5 minutes, equilibrate to 5°C for five minutes, acquire for three hours; heat stepwise to 60°C equilibrating each 5°C-step for 5 minutes, acquire for three hours at the chosen temperatures. Each 3-hour measurement consisted of six individual measurements of 30 minutes, which were compared and summed. The analysis of the SAXS spectra was carried out through GAP, Global Analysis Program, generously provided by Georg Pabst[31,32] (Institute of Biophysics and Nanosystems Research, Austrian Academy of Sciences Graz, Austria), choosing the paracrystalline theory as model of the structure factor. This approach allows an accurate evaluation of the lamellar phase structural parameter (d, smectic period d_B bilayer thickness), while the accuracy of the absolute values of the bilayers' internal parameters (d_c lipid chain thickness along the z-axis) should be taken with due caution, both for the intrinsic limitations of the model [31,32] and for the quality of the experimental data, in terms of peak width and number of reflections observed.

Confocal Laser Scanning Microscopy: CLSM experiments were carried out with a confocal laser scanning microscope Leica TCS SP2 (Leica Microsystems GmbH, Wetzlar, Germany) equipped with a 63x water immersion objective instrument by using 488-nm (NBD-PE) and 561-nm (Liss Rhod PE) laser lines. 70 μl of GUV solution in Sucrose 15mM was put in a chamber and then diluted adding 180 μl of Glucose 15mM. 100 μl of lipoplexes' dispersion stained with NBD-PE liposomes were prepared as previously described, incubated at room temperature for 20 minutes and then added to GUV solutions in the chambers. Samples containing lipoplexes and GUV were incubated for two hours respectively at 25°C and at 37°C before the acquisition of the images.

Results and Discussion

Thermal and structural properties of EDPPC/zwitterionic lipid bilayers.

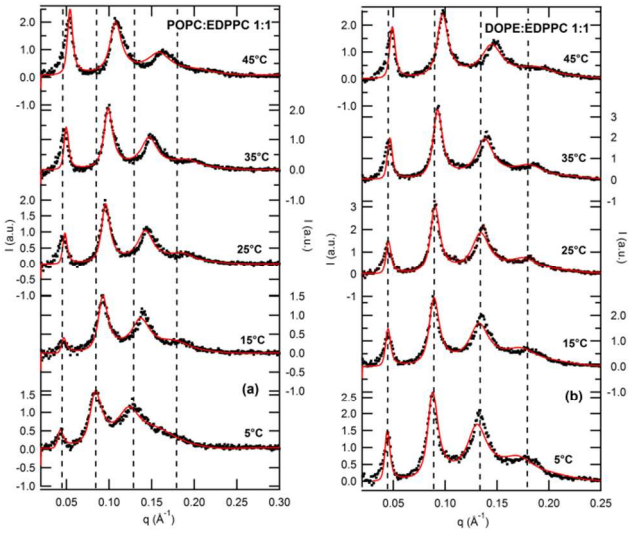

Fig. 2 SAXS spectra at 5°C, 15°C, 25°C, 35°C, 45°C (black dotted lines): (a) POPC:EDPPC 1:1 MLV and (b) DOPE:EDPPC 1:1 MLV; red lines are obtained from the analysis with Global analysis method according to a paracrystalline theory model fit.

Ethylphosphocholine liposomes have been proposed as DNA vectors in formulations differing for the length and saturation of the acyl chains. Interestingly, liposomes from a blend of ethylphosphocholines with different acyl chains showed a higher transfection efficiency than those containing a single type of hydrophobic chain.[33] This effect was related to the phase properties of the lipid membranes, and in particular to the large gel-liquid crystalline coexistence region, which in turn affects membrane fluctuations, permeability and fusogenicity at physiological temperatures.[34,35]

EDPPC has two saturated carbon chains, and, when fully hydrated, it assembles in an interdigitated bilayer in the gel phase at room temperature. The interdigitated bilayer undergoes a sharp $L_{\beta I}$-L_α transition[19] at 42°C (ΔH= 9.6 kcal/mol), as shown in the DSC thermogram reported in Figure 1. POPC and DOPE bilayers are instead characterized by a gel to liquid crystalline L_β-L_α transition below room temperature (T_m (POPC) = -2.5°C, ΔH = 5.8 kcal/mol;[36] T_m (DOPE) = -7.3°C, ΔH = 4.5 kcal/mol[37]) with an additional liquid crystalline-inverse hexagonal transition for DOPE at 5°C, due to the negative spontaneous curvature.[38] Figure 1 displays the thermograms of POPC:EDPPC 1:1 and DOPE:EDPPC 1:1 multilamellar bilayers in water excess. Both profiles are characterized by the presence of two distinct peaks for the gel to liquid crystalline transition, indicating a demixing of EDPPC with both zwitterionic lipids.

Previous studies on mixed EDPPC/DPPC have shown a thermotropic ideal behaviour for a wide range of mole ratios;[19] therefore the phase coexistence observed is related to the *cis*-unsaturations of the phospholipids, which affect the packing of the hydrocarbon chains in the mixed bilayer, determining the formation of separated domains.

In particular, the DSC profile of POPC:EDPPC is characterized by two broad peaks of comparable amplitudes at intermediate temperatures (15°C and 30°C) with respect to the transitions of the pure lipids, consistent with the formation of separated domains enriched in POPC, with lower L_β-L_α transition temperature, coexisting with bilayers enriched in EDPPC.

DOPE:EDPPC 1:1 bilayers are instead characterized by an intense and broad transition at 25°C and a weaker peak, occurring at a temperature very close to the transition of pure EDPPC. Similarly to what previously observed for EDMPC-DOPE mixtures,[27] this effect can be ascribed to the presence of a residual excess of pure EDPP domains coexisting with a mixture of EDPPC-DOPE, slightly enriched in DOPE.

Therefore, while EDPPC has a nearly ideal mixing behaviour with DOPE, the 1:1 mixture with POPC consists of two different phases with distinct fluidity at room temperature. The gel regions are enriched in EDPPC and feature a higher positive charge density than the fluid bilayers. This behaviour has possible consequences in the complexation of DNA, where electrostatic compensation is the driving force, and in the colloidal stability both of liposomal dispersion and of lipoplexes.

SAXS and WAXS measurements at different temperatures were performed to shed light on the structural properties of the bilayers. Figure 2 shows the SAXS spectra of POPC:EDPPC 1:1 and DOPE:EDPPC 1:1 MLVs. Irrespectively of the nature of the helper lipid, and in particular of its spontaneous curvature, both mixtures are arranged in a well ordered lamellar phase, characterized by the presence of at least four Bragg reflections.

The polar headgroup of EDPPC, upon the phosphate esterification, is more bulky with respect to DPPC, the non-esterified phosphocholine, due to combined steric and electrostatic effects.[27] Therefore the lipid has a positive spontaneous curvature, which matches the curvature of DOPE, resulting in a balanced planar bilayer.

In addition, SAXS does not evidence the coexistence of multiple smectic phases: irrespectively of the temperature we observe only one series of lamellar reflection. This means that there is no long-range correlation of the domains along the bilayer normal. A long-range order of lipid domains on the z-axis has been reported for DOPC-sphingomyelin-cholesterol lamellar phases, which are generally employed as mimic systems for cell membrane lipid rafts.[39] The spontaneous stacking of EDPPC-rich domains of adjacent bilayers is prevented by the electrostatic repulsion caused by the net positive charge of the domains.. The SAXS profiles can be therefore related to lamellae where the structure of EDPPC-rich and EDPPC-poor domains is averaged.

The red lines in Figure 2 represent the curve fitting obtained through the Global analysis method, which yields a Gaussian model representation of the bilayer electron density profiles and an estimate of the trend of the bilayer structural parameters with temperature increase, reported in Figure 3. The electronic density profile is related to the inner structure of the bilayer: in particular the minimum is located in correspondence of the terminal methyl groups, while the two maxima identify the phosphate head group of the lipids.

For both mixtures, an increase of temperature causes the contraction of the bilayer thickness (d_B), as shown by the comparison of the electron density profiles. The transition from a gel to a liquid crystalline phase is generally accompanied by a decrease of the bilayer thickness; for the gel interdigitated phase,

Cite this: DOI: 10.1039/c0xx00000x

www.rsc.org/xxxxxx

ARTICLE TYPE

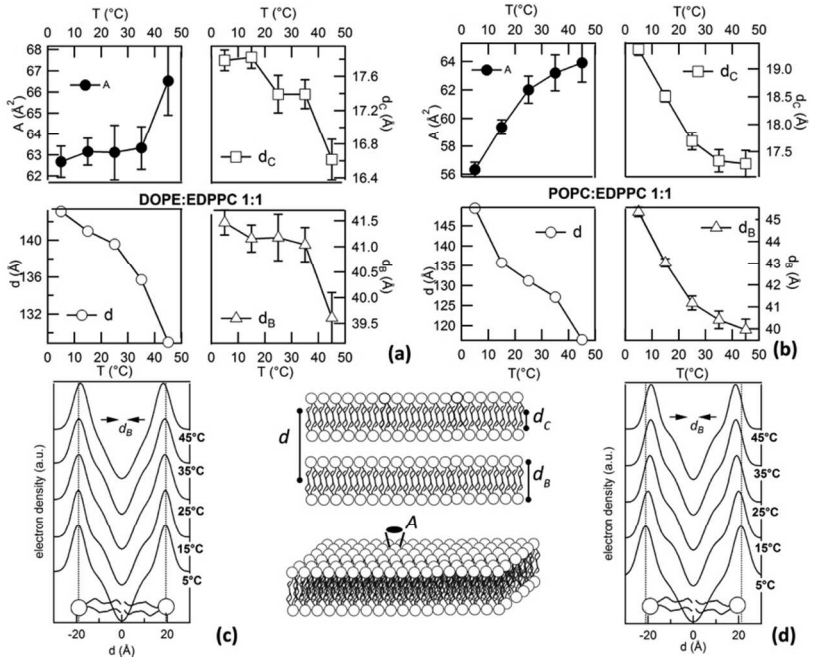

Fig. 3 Trend of DOPE:EDPPC 1:1 MLV (a) and POPC:EDPPC 1:1 MLV (b) bilayer structural parameters, as represented in the central scheme, obtained from the fitting procedure of SAXS spectra with the increase of temperature (5°C, 15°C, 25°C, 35°C, 45°C): d (Å) bilayer spacing or smectic period of the lamellar phase (empty circles), d_B (Å) bilayer thickness (empty triangles), d_C (Å) lipid chain thickness within the bilayer (empty squares), A (Å^2) polar headgroup averaged surface area (filled circles) estimated as $A = 2V_l / d_B$ with V_l lipid molecular volume obtained from phosphatidylcholine submolecular fragment volumes determined by Armen et al.[41] through molecular dynamic simulations. Gaussian model for the electron density profile of the bilayer along the z-axis, being the bilayer thickness (d_B) corresponding to the distance between the two opposed electron density maxima, (c) DOPE:EDPPC 1:1 MLV and (d) POPC:EDPPC 1:1 MLV at increasing temperatures.

melting can determine a slight increase in d_B, due to the opposed effect of the interdigitation loss and fluidity increase, as observed for pure EDPPC.[40]

Our results are consistent with the fact that mixing with POPC and DOPE prevents the interdigitated arrangement in the gel phase, due to the hindrance mismatch of the different chains. As the temperature increases, the smectic period of the lamellar stacks d , the bilayer thickness d_B and the lipid chain thickness within the bilayer d_C decrease, while at the same time the surface area A of the polar headgroup increases, as reported in Figures 3a and 3b.

This trend of the bilayer parameters is due to the transition from a gel state to a liquid crystalline one, that increases the mobility and the extent of gauche-trans isomerization for the lipid chains within the membrane, resulting in a general decrease of the bilayer thickness and in a larger hydration of the polar headgroups, i.e. in a larger cross section per lipid molecule.

These variations can be closely related to the DSC thermograms measured for the same lipid mixtures. The major changes in the membrane parameters are observed between 35°C and 45°C for DOPE:EDPPC 1:1 and below 25°C (in particular between 5°C and 15°C) for POPC:EDPPC 1:1, corresponding to the phase transition regions.

The comparison of the two formulations indicates that at the biologically relevant temperature, 37°C, the EDPPC:POPC mixture is in the fluid phase, while EDPPC:DOPE still contains domains of almost pure EDPPC in the gel phase.

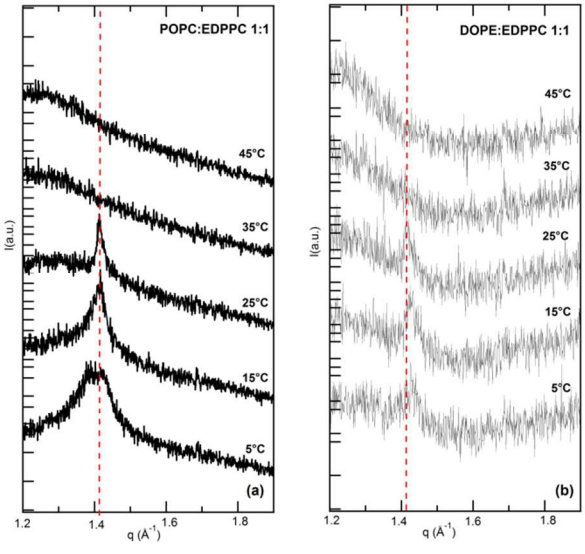

Fig. 4 WAXS spectra at 5°C, 15°C, 25°C, 35°C, 45°C: (a) POPC:EDPPC 1:1 MLV and (b) DOPE:EDPPC 1:1 MLV.

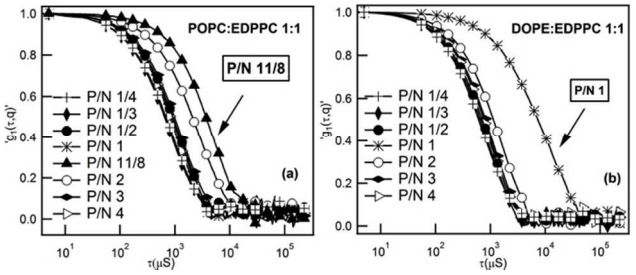

Fig. 5 Autocorrelation Functions of scattering intensity measured at 90°for DNA 5x10^{-5} M and (a) POPC:EDPPC 1:1 and (b) DOPE:EDPPC 1:1 from 1/4 to 4 P/N ratios in Hepes 10mM pH 7.4.

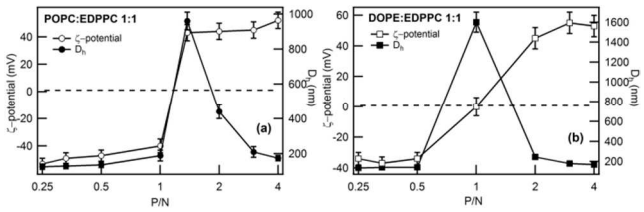

Fig. 6 Mean hydrodynamic diameter and zeta potential values (filled and open markers) versus the P/N ratio: (a) POPC:EDPPC 1:1 and (b) DOPE:EDPPC 1:1 lipoplexes.

The WAXS spectra, displayed in Figure 4a and 4b, are in perfect agreement with the previous experiments. At low temperatures both MLVs show a peak around q = 1.45 Å^{-1}, indicating the typical in-plane correlation of a gel phase (L_β) that disappears when the temperature is raised towards the liquid crystalline phase. In particular, the WAXS reflection of POPC:EDPPC 1:1 at 5°C clearly results from the superposition of two in-plane correlations, indicating the presence of two distinct phases that coexist in the same bilayer. At 15°C the peak profile narrows and becomes sharp at 25°C, highlighting the melting transition.

The WAXS spectra measured at 35°C and at 45°C are identical, with the disappearance of the L_β peak and the appearance of a broad peak of the L_α phase at q= 1.2 Å^{-1}, in agreement with DSC. Conversely, for DOPE:EDPPC, the WAXS spectra (Figure 3a) show a low intensity L_β peak, which is partially hidden in the background, at 35°C, confirming the presence of a residual bilayer portion enriched in EDPPC within the bilayer, responsible for the higher transition temperature observed in the corresponding thermogram.

The disappearance of the L_β peak in the WAXS spectra of both mixtures is gradual. This behaviour, in agreement with the SAXS and DSC data previously discussed, is consistent with a large temperature interval, where the phase domains with different lipid compositions and charge density coexist in the same bilayer. This lateral inhomogeneity can affect both DNA complexation and properties of the complexes in terms of fusogenic efficiency with target bilayers.

DNA complexation of EDPPC-based liposomes.

DLS and Zeta Potential were performed to monitor DNA complexation by POPC:EDPPC and DOPE:EDPPC unilamellar liposomes. The unilamellar liposomes obtained by extrusion have hydrodynamic diameters of 93 nm and 97 nm, respectively, with extremely low polydispersity (0.046 and 0.072 respectively (SI Figure 1)). The zeta potential values (+57 ± 4 mV for both liposomes) indicate a net positive charge density. We recall however that, due to lipid demixing, the positive charge is not homogeneously distributed in the bilayer.

The dispersions were then added in different amounts to DNA solution, to vary the charge ratio P/N (stoichiometric ratio of positive to negative charges). Figure 5a and 5b show the autocorrelation functions (ACFs) of the scattered intensity for POPC:EDPPC and DOPE:EDPPC liposomes/DNA, as P/N is increased. The progression of the autocorrelation function is consistent with an increase of hydrodynamic size, due to the formation of lipoplexes. This evidence is paralleled by the CD results (SI Figure 2), which indicate the compaction of DNA in a condensed *psi*-like form[42,43] upon interaction with cationic liposomes.

Figure 6a and 6b compare the trend of zeta potential to the hydrodynamic size of the complexes as P/N is increased. At P/N = 1/4 the zeta potential is strongly negative for both lipoplexes, indicating that DNA in excess coats the liposomal surface. As P/N increases, the zeta potential becomes less negative, until P/N~1, where the overall charge reverses, turning positive. Eventually, for P/N >2, the zeta potential oscillates around an equilibrium positive value. In parallel, the hydrodynamic diameter of lipoplexes first increases, reaching a maximum around the zero-charge point, and then decreases for P/N values larger than 1. This behaviour is characteristic of the so-called reentrant condensation:[44,45] the isoelectric point corresponds to the minimal electrostatic repulsion between lipoplexes, which clusterize reaching the maximum hydrodynamic size. Interestingly, the reentrant condensation curve is shifted at higher P/N values for POPC:EDPPC lipoplexes, which reach the isoelectric point at P/N=11/8, with respect to DOPE:EDPPC (whose charge reverses at P/N = 1).

This effect can be explained considering the DSC and SAXS results on POPC:EDPPC at 25°C, which highlighted a phase separation in domains containing different amounts of EDPPC. The bilayers contain patches of variable surface charge, which determine an additional attractive contribution to the clusterization of lipoplexes, driven by the surface charge inhomogeneity, according to the Thwar-Velegol charge patch attraction model.[46,45]

DOPE:EDPPC bilayers at the same temperature are instead characterized by a comparatively low excess of pure EDPPC with respect to stoichiometric mixing, thus, the Thwar-Velegol contribution to clusterization is lower.

The balance between lipoplex size and charge is key in the development of efficient DNA non viral vectors for gene therapy, both in terms of transfection efficiency and cytotoxicity of lipoplexes.[47,48]

In summary, the reentrant condensation provides key information to tune both transfection efficiency and biocompatibility of the vectors. Moreover, the higher quantity of POPC:EDPPC liposomes (the vector) necessary to reach the isoelectric point in the presence of the same amount of DNA (the designed genetic drug), i.e. P/N=11/8 with respect to DOPE:EDPPC liposomes (P/N=1), reveals a higher efficiency of the latter system in the binding and encapsulation of DNA.

The observed differences in the reentrant condensation profile follows from the different structural properties of the bilayers, and in particular lipid demixing induced by POPC. DNA binding

Cite this: DOI: 10.1039/c0xx00000x

www.rsc.org/xxxxxx

ARTICLE TYPE

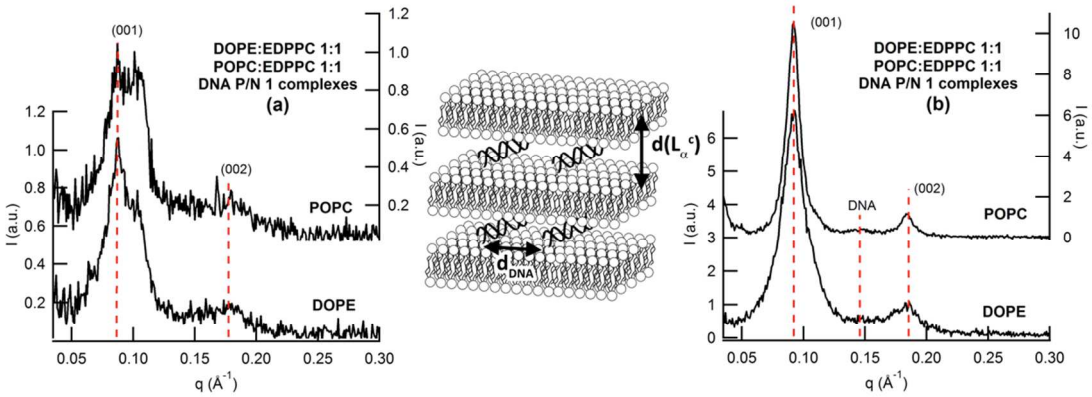

Fig. 7 SAXS spectra acquired for POPC:EDPPC 1:1-DNA P/N=1 and DOPE:EDPPC 1:1-DNA P/N=1 lipoplexes at 25°C: (a) lipoplexes incubated at room temperature for 24 h before measurement (b) lipoplexes incubated at 40°C for 24 h before measurement with the scheme in the middle sketching their hypothesized structure.

is affected by the lipid phase behaviour, suggesting DOPE as a better helper lipid to obtain a better encapsulation of DNA in the lipoplexes.

Effects of the thermal treatment of the samples on the internal structure of lipoplexes.

To further address the effect of the phase state on the structure and composition of the complexes, we have compared lipoplexes with the same lipid and DNA concentrations at different temperatures, 25°C and 37°C, where EDPPC:POPC bilayers are homogeneous, while DOPE:EDPPC still exhibits residual domains of pure EDPPC.

Figure 7a shows the SAXS spectra measured at 25°C for POPC:EDPPC and DOPE:EDPPC lipoplexes (P/N=1) incubated at room temperature. Upon complexation with DNA, both kind of unilamellar liposomes form lipoplexes with an internal lamellar structure, characterized by identical smectic spacing, 70.8 Å. At q = 0.102 Å^{-1} a third reflection that cannot be assigned to the main lamellar phase, appears close to the intense first order Bragg reflection from the stacked bilayers, which can be related to the presence of a second lamellar phase, with spacing of 61-62 Å, induced by DNA complexation. The SAXS patterns are very similar, highlighting that the structural organization is basically driven by the cationic lipid EDPPC. The thinner lamellar phase can be thought to arise from lateral phase separation in a gel state, induced by DNA binding, which has been observed in some other cases for lipid/DNA complexes.[49,50]

Figure 7b displays the SAXS from POPC:EDPPC 1:1 and DOPE:EDPPC 1:1 lipoplexes (P/N=1) prepared pre-incubating at 37°C for 24 hours both DNA and MLVs before adding the multilamellar vesicles to the nucleic acid solution. The complexes were then further incubated at 37°C for one hour before measurement, performed at 25°C, in the same experimental conditions as the previous set of samples. The lipoplexes are much more ordered and laterally homogeneous. The extra-lamellar peak is related to the in-plane correlation of DNA sandwiched between the bilayers.[51] The SAXS results indicate the presence of a single lamellar phases, characterized by the same smectic period of the lipoplexes at 25°C (70.8 Å) (Figure 7a). The in-plane correlation of DNA (q = 0.144 Å^{-1}), though very broad, corresponds to the interaxial spacing of a 1D lattice of DNA chains sandwiched between the lipid bilayers. This distance can be evaluated[52] as $d_{DNA} = 2\pi/q_{DNA}$, yielding 43.6 Å ($q_{DNA} \approx 0{,}144$ Å^{-1}).[53] The variations in the DNA interaxial spacing, i.e. the amount of DNA sandwiched within the lamellae, are related to the efficiency of the electrostatic compensation between the polyanionic DNA and the cationic polar headgroups on the liposomal surface.[54,55]

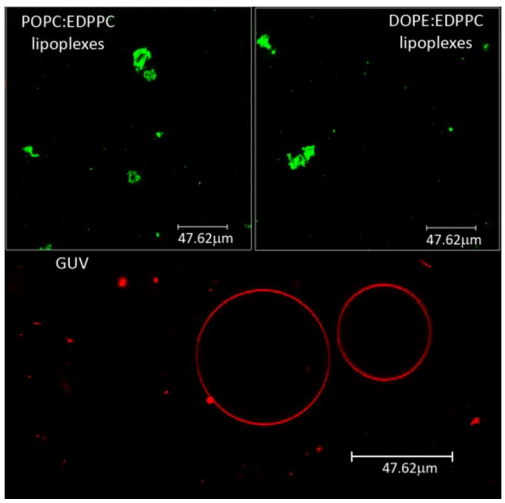

Fig. 8 CLSM images acquired for POPC:EDPPC 1:1 and DOPE:EDPPC 1:1 lipoplexes stained with NBD-PE (NBD-PE fluorescence in green) and for POPC GUV stained with LissRhod PE (LissRhod PE fluorescence in red).

Cite this: DOI: 10.1039/c0xx00000x

www.rsc.org/xxxxxx

ARTICLE TYPE

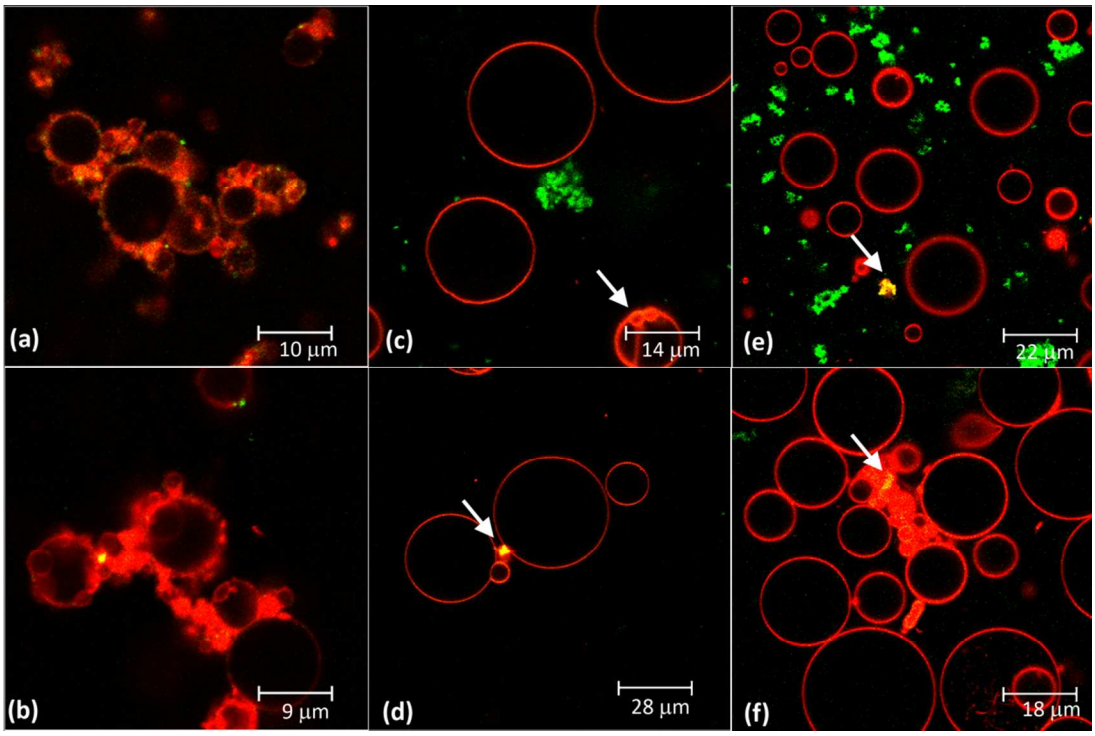

Fig. 9 CLSM images acquired for POPC:EDPPC 1:1 (a, c, e) DOPE:EDPPC 1:1 (b, d, f) lipoplexes stained with NBD-PE (NBD-PE fluorescence in green) incubated for two hours with: (a,b) POPG:POPC 1:1 anionic GUVs at 25°C; (c,d) POPC zwitterionic GUVs at 25°C; (e,f) POPC zwitterionic GUVs at 37°C. GUVs were stained with LissRhod PE (LissRhod PE fluorescence in red) and fluorescent probes' emission overlap is highlighted in yellow. White arrows in (c-f images) indicate the points where interaction between lipoplexes and GUVs appears evident.

The phase state of lipoplexes and of the bilayer changes drastically with the incubation temperature, both for POPC:EDPPC and for DOPE:EDPPC liposomes, possibly due to a reorganization of the lipid structure in the fluid phase upon annealing.

Overall, DLS and SAXS results highlight a non trivial role of lipid demixing and of the phase state for DNA complexation. The inclusion of unsaturated zwitterionic lipids in the formulation play a dual role, since both the lateral charge inhomogeneities and the fluidity of the mixed membranes appear as critical factors for DNA binding.

Interaction of lamellar lipoplexes with model membranes.

A key feature for transfection is the ability of the lipoplex to interact with cell membranes and to release the therapeutic principle inside the cytoplasm.

The surface docking of lipoplexes on the external cell membrane is the first step towards the activation of the endocytic pathway for internalization, with inclusion of the lipoplex in endosomes. The electrostatic driving force between the cationic lipoplexes and the negatively charged cell membrane is key for uptake and transfection.[56,57]

The endosomal escape of the lipid-DNA complexes is believed to be highly dependent on the ability of the lipoplexes to fuse with the endosomal membrane. In this latter process, the polymorphism of lipoplexes, provided e.g. by the addition of helper lipids with negative spontaneous curvature like DOPE, has been established as crucial in the enhancement of transfection.[58,57] As previously discussed, the hindrance of the EDPPC headgroup drives the formation of a lamellar phase for the complexes, irrespectively of the helper lipid. However, phase defects, due to non-ideal lipid mixing lipids in the membrane is recognized as a fusogenic factor for ethylphosphocholines, which enhances the transfection efficiency.[33]

To address this issue, we investigate for the first time the interaction of cationic EDPPC:DOPE 1:1 and EDPPC:POPC 1:1 lipoplexes (P/N=4) with anionic and zwitterionic Giant Unilamellar Vesicles (GUVs) at 25°C. At this temperature both liposomes are characterized by the presence of domains, conversely at 37°C (the biologically relevant temperature for transfection), POPC:EDPPC is homogeneously in the fluid phase, while DOPE:EDPPC exhibit the presence of EDPPC domains in the interdigitated gel phase, which can be assimilated to membrane defects. GUVs are reliable model membranes, employed to investigate biologically relevant phenomena that involve the plasma membrane, such as membrane fusion, cell uptake and trafficking processes, raft-like domains structure, membrane proteins specific functions.[59,28,60–62]

The interaction between GUVs (stained with the fluorescent lipid Liss-Rhod PE, Figure 8, lower panel) and lipoplexes (labelled

with NBD-PE, Figure 8, upper panels) has been visualized with CLSM (Confocal Laser Scanning Microscopy). For the lipoplex samples, large aggregates with diameters of some microns can be detected, consistently with the appearance of some precipitate one hour after mixing.

In order to assess the electrostatic contribution to the interaction, the cationic lipoplexes, containing DOPE or POPC as helper lipids, were incubated for two hours with anionic POPG:POPC 1:1 GUVs at 25°C. In this case, the confocal microscopy images (Figure 9a and 9b) highlight a clusterization of several GUVs, due to the bridging effect operated by the cationic lipoplexes, which crowd the membranes and appear as protrusions of the bilayer. In addition, an extended exchange of the fluorescent probes originally residing in the GUVs' bilayer (red) and lipoplexes (green) is highlighted by the wide regions of colocalization of their fluorescence emissions (yellow), suggesting the occurrence of membrane fusion between the lipoplexes and the target bilayers, which causes a cross-migration of the relative fluorescent tags.

The electrostatic attractive interaction is thus the major thermodynamic drive: it is worthwhile to stress that natural membranes are generally negatively charged; therefore our observation is in line with the requirement that lipoplexes should have a positive zeta potential.[57]

At this stage, no clear differentiation between the two DNA vectors emerge. To verify the presence of additional subtler contributions, the same cationic lipoplexes were incubated with uncharged POPC GUVs at 25°C (Figure 9c and 9d) and at 37°C (Figure 9e and 9f).

If the target membrane is zwitterionic rather than anionic, and the incubation between lipoplexes and GUVs is carried out at 25°C (Figure 9c and 9e) the interaction results attenuated, confirming the fact that the electrostatic contribution is the dominant contribution; however, also in this case some fusion events (highlighted by the white arrows in the images) can be detected, indicating a possible additional driving force, which could play a role in the fusogenic ability and could be identified in the presence of structural defects within the lipid membrane, detected in these membranes with DSC, SAXS and WAXS.

Interestingly, when the incubation of cationic lipoplexes and uncharged GUVs is performed at a higher temperature (37°C), a different behaviour is observed for EDPPC:POPC and EDPPC:DOPE lipoplexes. An enhancement of fusion events, possibly due to the higher mobility of the lipoplexes is observed only for the vectors containing DOPE. Conversely, no meaningful difference between 25°C and at 37°C can be appreciated for POPC lipoplexes. Figure 9f shows the presence of extended clusterization provoked by the presence of DOPE:EDPPC lipoplexes, and wide regions of colocalization for the lipid tags originally separated in the GUV bilayer and lipoplexes. We might speculate on this effect and attribute it to the different structure of the lipid bilayers at 37°C. The disappearance of the structural defects in POPC:EDPPC at 37°C (completely in the fluid phase) possibly decreases the affinity for the target bilayer, contrasting the effect of a temperature increase. In the same temperature range DOPE:EDPPC bilayers still contains gel domains with an EDPPC excess within the membrane. The combination between temperature increase and the presence of structural defects, determines an increase of fusogenic ability, with respect to what observed at 25°C.

Conclusions

In this paper we investigate the effect that the inclusion of zwitterionic helper lipids on EDPPC-based liposomes designed as DNA vectors. A peculiar role of the helper lipids added to EDPPC (DOPE and POPC) emerges, not only due to the tuning of the surface charge density, but also to lipid demixing which results in laterally separated domains with a complex thermotropic phase behaviour. The mixed bilayers are characterized by the presence of coexisting domains in a wide temperature range around the physiologically relevant temperature

The reentrant condensation exhibited by the lipoplexes depends on the phase state of the bilayers.

The fusogenic ability, crucial for the interaction between lipoplexes and membranes, has been investigated in model systems as a function of temperature. Interestingly, the interaction with target membranes, is enhanced by the presence of gel domains coexisting with fluid domains in the biologically relevant temperature range.

Acknowledgements

The authors acknowledge financial support from MIUR under the projects PRIN 2010-2011(2010BJ23MN) and FIRB RBPR05JH2P_007 ITALNANONET.

Notes and references

[a] *CSGI and Department of Chemistry, University of Florence, via della Lastruccia 3, 50019, Sesto Fiorentino, Firenze, Italy. Fax: +390554573036; Tel: +39 055 4573017, E-mail: montis@csgi.unifi.it; Tel: +39 055 4573033, E-mail: baglioni@csgi.unifi.it; * Tel: +39 055 4573038, E-mail: berti@csgi.unifi.it*

[b] *Present address: Institut für Zelluläre und Molekulare Physiologie, Friedrich-Alexander-Universität Erlangen-Nürnberg, Waldrstrasse 6. 91054 Erlangen, German. E-mail: silvia_sostegni@virgilio.it.*

[c] *Present address: Soft Condensed Matter Group, Faculty of Physics, Ludwig-Maximilian-Universität, Geschwister Scholl Platz 1, 80539 München, Germany. E-mail: Silvia.Milani@physik.uni-muenchen.de.*

† Electronic Supplementary Information (ESI) available: [additional experimental Dynamic Light Scattering and Circular Dichroism data]. See DOI: 10.1039/b000000x/

1. C. Uherek and W. Wels, *Adv. Drug Deliv. Rev.*, 2000, **44**, 153–166.
2. W. A. Denny, *J. Biomed. Biotechnol.*, 2003, 48–70.
3. S. T. Crooke, *Biochim. Biophys. Acta-Gene Struct. Expr.*, 1999, **1489**, 31–44.
4. A. C. Yan and M. Levy, *Rna Biol.*, 2009, **6**, 316–320.
5. R. Juliano, J. Bauman, H. Kang, and X. Ming, *Mol. Pharm.*, 2009, **6**, 686–695.
6. C. Mah, B. J. Byrne, and T. R. Flotte, *Clin. Pharmacokinet.*, 2002, **41**, 901–911.
7. T. L. Timme, S. J. Hall, R. Barrios, S. L. C. Woo, E. Aguilar-Cordova, and T. C. Thompson, *Cancer Gene Ther.*, 1998, **5**, 74–82.
8. C. R. Safinya, K. Ewert, A. Ahmad, H. M. Evans, U. Raviv, D. J. Needleman, A. J. Lin, N. L. Slack, C. George, and C. E. Samuel, *Philos. Trans. R. Soc. a-Mathematical Phys. Eng. Sci.*, 2006, **364**, 2573–2596.
9. V. a Bloomfield, *Curr. Opin. Struct. Biol.*, 1996, **6**, 334–41.
10. S. Dokka, D. Toledo, X. G. Shi, V. Castranova, and Y. Rojanasakul, *Pharm. Res.*, 2000, **17**, 521–525.

11. R. C. MacDonald, V. a Rakhmanova, K. L. Choi, H. S. Rosenzweig, and M. K. Lahiri, *J. Pharm. Sci.*, 1999, **88**, 896–904.
12. R. J. McDonald, H. D. Liggitt, L. Roche, H. T. Nguyen, R. Pearlman, O. G. Raabe, L. B. Bussey, and C. M. Gorman, *Pharm. Res.*, 1998, **15**, 671–679.
13. C. M. Gorman, M. Aikawa, B. Fox, E. Fox, C. Lapuz, B. Michaud, H. Nguyen, E. Roche, T. Sawa, and J. P. Wiener-Kronish, *Gene Ther.*, 1997, **4**, 983–92.
14. S. Duarte, H. Faneca, and M. C. P. De Lima, *Int. J. Pharm.*, 2012, **423**, 365–77.
15. C. Barnier Quer, A. Elsharkawy, S. Romeijn, A. Kros, and W. Jiskoot, *Eur. J. Pharm. Biopharm.*, 2012, 81, 294–302.
16. G. Shim, H.-W. Choi, S. Lee, J. Choi, Y. H. Yu, D.-E. Park, Y. Choi, C.-W. Kim, and Y.-K. Oh, *Mol. Ther.*, 2013, **21**, 816–24.
17. B. Tenchov, Y. Sugimoto, R. Koynova, R. W. Brueggemeier, and R. J. Lee, *Anticancer Res.*, 2012, **32**, 2563–6.
18. R. Koynova, B. Tenchov, L. Wang, and R. C. MacDonald, *Mol. Pharm.*, 2009, **6**, 951–958.
19. R. Koynova and R. C. MacDonald, *Biophys. J.*, 2003, **85**, 2449–65.
20. R. Koynova, Y. S. Tarahovsky, L. Wang, and R. C. MacDonald, *Biochim. Biophys. Acta*, 2007, **1768**, 375–86.
21. J. Rejman, G. Tavernier, N. Bavarsad, J. Demeester, and S. C. De Smedt, *J. Control. Release*, 2010, **147**, 385–91.
22. Z. Y. He, X. Zheng, X. H. Wu, X. R. Song, G. He, W. F. Wu, S. Yu, S. J. Mao, and Y. Q. Wei, *Int. J. Pharm.*, 2010, **397**, 147–54.
23. D. K. Jensen, L. B. Jensen, S. Koocheki, L. Bengtson, D. Cun, H. M. Nielsen, and C. Foged, *J. Control. Release*, 2012, **157**, 141–8.
24. R. Kedmi, N. Ben-Arie, and D. Peer, *Biomaterials*, 2010, **31**, 6867–75.
25. Y.-D. Sohn, I. Somasuntharam, P.-L. Che, R. Jayswal, N. Murthy, M. E. Davis, and Y. Yoon, *Biomaterials*, 2013, **34**, 4235–41.
26. R. Labas, F. Beilvert, B. Barteau, S. David, R. Chèvre, and B. Pitard, *Genetica*, 2010, **138**, 153–168.
27. M. Saunders, K. M. G. Taylor, D. Q. M. Craig, K. Palin, and H. Robson, *Pharm. Res.*, 2007, **24**, 1954–1961.
28. M. I. Angelova, S. Soleau, P. Meleard, J. F. Faucon, and P. Bothorel, *Trends Colloid Interface Sci. Vi*, 1992, **89**, 127–131.
29. S. Nappini, T. Al Kayal, D. Berti, B. Norden, and P. Baglioni, *J. Phys. Chem. Lett.*, 2011, **2**, 713–718.
30. C. Montis, S. Milani, D. Berti, and P. Baglioni, *J. Colloid Interface Sci.*, 2012, **373**, 57–68.
31. G. Pabst, M. Rappolt, H. Amenitsch, and P. Laggner, *Phys. Rev. E*, 2000, **62**, 4000–4009.
32. G. Pabst, R. Koschuch, B. Pozo-Navas, M. Rappolt, K. Lohner, and P. Laggner, *J. Appl. Crystallogr.*, 2003, **36**, 1378–1388.
33. L. Wang and R. MacDonald, *Mol. Pharm.*, 2007, **4**, 615–623.
34. D. Marsh, A. Watts, and P. F. Knowles, *Biochemistry*, 1976, **15**, 3570–3578.
35. J. Lemmich, K. Mortensen, J. Ipsen, and T. Hønger, *Phys. Rev. Lett.*, 1995, **75**, 3958–3962.
36. R. Koynova and M. Caffrey, *Biochim. Biophys. Acta*, 1998, **1376**, 91–145.
37. R. Koynova and M. Caffrey, *Chem. Phys. Lipids*, 1994, **69**, 1–34.
38. G. E. S. Toombes, A. C. Finnefrock, M. W. Tate, and S. M. Gruner, *Biophys. J.*, 2002, **82**, 2504–2510.
39. L. Tayebi, Y. Ma, D. Vashaee, G. Chen, S. K. Sinha, and A. N. Parikh, *Nat. Mater.*, 2012.
40. I. Winter, G. Pabst, M. Rappolt, and K. Lohner, *Chem. Phys. Lipids*, 2001, **112**, 137–50.
41. R. S. Armen, O. D. Uitto, and S. E. Feller, *Biophys. J.*, 1998, **75**, 734–744.
42. D. Simberg, D. Danino, Y. Talmon, a Minsky, M. E. Ferrari, C. J. Wheeler, and Y. Barenholz, *J. Biol. Chem.*, 2001, **276**, 47453–9.
43. B. B. Hopkins and N. O. Reich, *J. Biol. Chem.*, 2004, **279**, 37049–60.
44. S. Sennato, F. Bordi, C. Cametti, A. Diociaiuti, and P. Malaspina, *Biochim. Biophys. Acta-Biomembranes*, 2005, **1714**, 11–24.
45. S. Sennato, D. Truzzolillo, F. Bordi, F. Sciortino, and C. Cametti, *Colloids Surfaces a-Physicochemical Eng. Asp.*, 2009, **343**, 34–42.
46. D. Velegol and P. K. Thwar, *Langmuir*, 2001, **17**, 7687–7693.
47. I. Tranchant, B. Thompson, C. Nicolazzi, N. Mignet, and D. Scherman, *J. Gene Med.*, 2004, **6**, S24–S35.
48. C. R. Dass, *J. Mol. Med.*, 2004, **82**, 579–591.
49. D. Uhríková, N. Kučerka, A. Lengyel, P. Pullmannová, J. Teixeira, T. Murugova, S. S. Funari, and P. Balgavý, *J. Phys. Conf. Ser.*, 2012, 351, 012011.
50. P. Pullmannová, M. Bastos, G. Bai, S. S. Funari, I. Lacko, F. Devínsky, J. Teixeira, and D. Uhríková, *Biophys. Chem.*, 2012, 160, 35–45.
51. J. O. Radler, *Science (80-.).*, 1997, **275**, 810–814.
52. C. R. Safinya, *Curr. Opin. Struct. Biol.*, 2001, **11**, 440–448.
53. G. Caracciolo, D. Pozzi, H. Amenitsch, and R. Caminiti, *Langmuir*, 2005, **21**, 11582–11587.
54. C. Safinya, *Curr. Opin. Struct. Biol.*, 2001, 440–448.
55. J. McManus, J. Rädler, and K. Dawson, *Langmuir*, 2003, 9630–9637.
56. L. Wasungu and D. Hoekstra, *J. Control. Release*, 2006, **116**, 255–264.
57. I. S. Zuhorn, J. Engberts, and D. Hoekstra, *Eur. Biophys. J. with Biophys. Lett.*, 2007, **36**, 349–362.
58. I. S. Zuhorn, U. Bakowsky, E. Polushkin, W. H. Visser, M. C. A. Stuart, J. Engberts, and D. Hoekstra, *Mol. Ther.*, 2005, **11**, 801–810.
59. J. Korlach, P. Schwille, W. W. Webb, and G. W. Feigenson, *Proc. Natl. Acad. Sci. U. S. A.*, 1999, **96**, 9966.
60. R. Machán and M. Hof, *Biochim. Biophys. Acta*, 2010, **1798**, 1377–91.
61. P. Walde, K. Cosentino, H. Engel, and P. Stano, *Chembiochem*, 2010, **11**, 848–65.
62. C. Montis, P. Baglioni, and D. Berti, *Soft Matter*, 2014, **10**, 39.

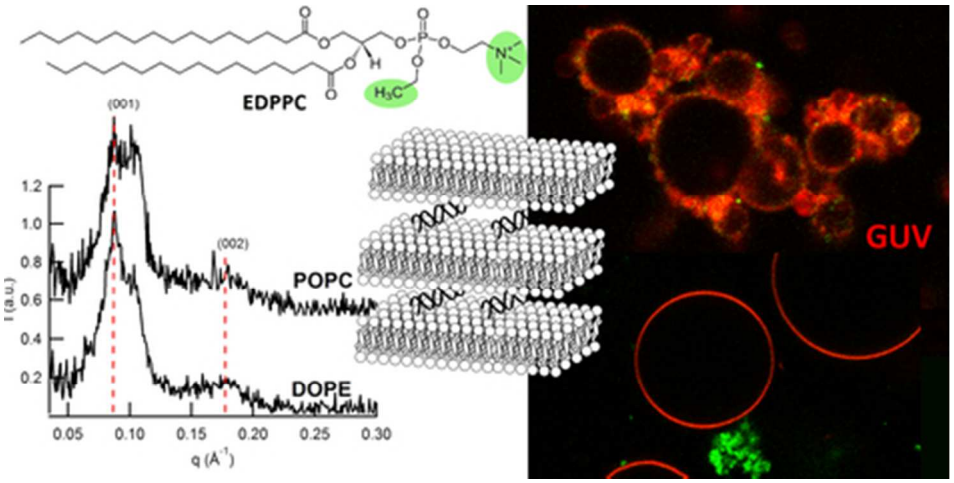

39x19mm (300 x 300 DPI)